JOURNAL OF CATALYSIS 48, 42–59 (1977)

The Relation of Surface Structure to the Electrocatalytic Activity of Tungsten Carbide

PHILIP N. ROSS, JR., AND PAUL STONEHART

Advanced Fuel Cell Research Laboratory, Power Systems Division, United Technologies Corporation, Middletown, Connecticut 06457

Received June 28, 1976; revised January 24, 1977

The electrocatalytic activities of high surface area tungsten carbides for H_2 oxidation in acid electrolytes were studied and found to be dependent on the methods of preparation of the carbides. Auger electron spectroscopy and X-ray photoemission spectroscopy were used to determine how the surface compositions and chemical states of surface atoms varied with methods of preparation. Bulk crystallographic structures were determined using X-ray diffraction. Low temperature (700°C) carburization of tungstic acid was found to deposit or cause the accumulation of an inert carbon layer over the tungsten carbide. This phenomenon could be minimized by mixing the tungstic acid with 10 w/o NH_4Cl. The most active carbide was slightly carbon deficient at both the surface and in the bulk, with the carbon deficiency probably replaced by oxygen. This active surface was most easily prepared by carburizing amorphous, white, tungstic acid hydrate. Oxygen substitution for carbon probably occurs during an intermediate state of carbon dissolution in the reduced tungsten metal and is aided by the defect structure in the tungstic acid. The increased activity of the oxygen substituted carbide is due to a reduced interaction of the surface with the electrolyte, resulting from covalent tungsten–oxygen bonding. The absolute activity of active tungsten carbide for the oxidation of pure H_2 at 25°C is four orders of magnitude lower than that for Pt.

INTRODUCTION

In the last decade, several laboratories engaged in fuel cell research have sought to develop an acid resistant catalyst that might replace platinum as the anode catalyst. In the acid electrolyte fuel cell anode, hydrogen is converted electrochemically according to the half-cell reaction,

$$H_2 \rightleftharpoons 2H^+ + 2e^-,$$

where H^+ represents the hydrogen ion in aqueous solution. Carbides, borides, nitrides and silicides of the transition metals have been investigated for their suitability and as electrode materials (*1–5*). Tungsten carbide, WC, is the most active of these alternatives for hydrogen oxidation in acid electrolyte, and is not poisoned at any level of carbon monoxide (*6*), nor by several volumes ppm hydrogen sulfide (*6*). The electrocatalytic activity of tungsten carbide has been demonstrated in numerous studies to depend greatly on the method of preparation (*5–9*). It has also been reported that the activity of WC can be improved by electrochemical activation, anodizing to 1 V [reversible hydrogen electrode (RHE) in the same electrolyte] in the presence of a reducing agent such as hydrogen or hydrazine (*10, 11*), or by mild gas-phase oxidation (*12*).

Tungsten carbide has also been reported as a catalyst for some gas-phase reactions. Levy and Boudart (*13*) reported that WC exhibited platinum-like behavior for H_2–O_2

ISSN 0021-9517

titration and isomerization of 2,3-dimethylpropane. The WC they examined was made by Dr. H. Boehm (AEG-Telefunken). Ross and Stonehart (*14*) investigated H_2–O_2 titration on several commercially available ultrahigh purity carbides (WC and W_2C) plus material from AEG-Telefunken and found only the AEG-Telefunken material catalyzed the titration reaction. These investigators also reported (*15*) that from the same group of carbides only the AEG-Telefunken WC and commercial W_2C had significant activity for the oxidation of H_2 in acid electrolyte.

In the present study, we relate the surface composition and structure to the method of preparation of the carbide, and in turn to the electrocatalytic activity of the carbide for hydrogen oxidation in acid. Auger electron spectroscopy (AES) is used to examine the composition of the surface, and X-ray photoemission spectroscopy (XPS) is used to examine the valence states of atoms at the surface. Neither of these techniques reflect the state of matter of just the outer monolayer of atoms. AES represents electron emission from the outermost 3–4 atomic layers, XPS from 5–10 atomic layers (*19*). Thus, the composition of a surface determined from AES does not necessarily represent the composition of the outermost layer of atoms, but rather, at best, represents an average composition of the first 3–4 atomic layers. Neither is it certain, however, that the catalytic properties of a surface are determined by only the outermost layer of atoms. It seems likely that the nature of the bonding of the first atomic layer to the second and third atomic layers of the catalyst surface is important in determining the catalytic properties of the surface. A spectroscopy like AES may, therefore, reflect composition changes within the surface region that determine the catalytic properties of materials.

EXPERIMENTAL METHODS

a. Preparation of High Surface Area tungsten Carbides

The unsupported carbides were all prepared by carburization of an intermediate oxide phase with carbon monoxide. The intermediate oxide phases were either yellow (crystalline), white (amorphous), or white (crystalline) modifications of tungstic acid hydrate ($WO_3 \cdot xH_2O$). They were precipitated from a concentrated aqueous solution of ammonium metatungstate (Baker Reagent Grade, purified by recrystallization) by the addition of a cold hydrochloric acid solution. The yellow modification resulted when concentrated HCl was added to make the solution pH < 2. The white modifications were precipitated when cold dilute HCl was added to make a solution of pH 5–6. The crystallinity of the white modification was controlled by varying the concentration of the ammonium metatungstate solution. The precipitates were separated by filtration, thoroughly washed with distilled water and dried in air at 120–140°C. The tungstic acid hydrates were carburized in a tube furnace with flowing carbon monoxide. The carburization temperatures were 600–900°C with the samples being rapidly heated to the carburization temperature in argon. The carburization time was optimized for each temperature to be the minimum time at each temperature necessary to convert all the oxide phase to the carbide form. For some of the samples, NH_4Cl was physically mixed with the tungstic acid hydrate prior to carburization as suggested by Svata and Zabransky (*8, 9*).

The crystallographic structures of the resulting tungsten carbides were determined by standard X-ray diffraction procedures. Direct current-arc emission spectrographic analysis confirmed that no Pt, Pd, Rh, or Ir was present above the lowest level of detection (2 ppm). The carbon contents of the carbides were determined by

the amount of CO_2 evolved on combustion. BET surface areas were determined using a Perkin–Elmer sorptometer.

Tungsten carbide supported on carbon black (Vulcan XC-72, Cabot Corp.) was prepared by impregnation from aqueous ammonium metatungstate solution. The tungsten complex was reduced by heating in flowing H_2 at 700°C for 2 hr to produce a supported tungsten metal intermediate, confirmed by X-ray diffraction. The carbon was diffused into the tungsten metal by further heating of the intermediate in argon for 30 hr at 1000°C. The carbide phases were identified by X-ray diffraction. Only a pure WC phase was observed, except when the tungsten content of the impregnated carbon exceeded 85 w/o, when a pure W_2C phase could be produced. Thus, two kinds of supported catalysts were prepared, one with single phase WC particles, one with single phase W_2C particles dispersed on the carbon black surface. The surface areas of the carbide phases were determined by particle size measurement using electron microscopy.

Nonporous (99% of theoretical density) rods of single phase WC and α-W_2C, to serve as analytical standards for Auger electron spectroscopy, were prepared by hot pressing stoichiometric mixtures of the elements at 2000°C for 12 hr.

b. *Surface Analysis of the Unsupported Tungsten Carbides*

The surface compositions of the unsupported tungsten carbides were analyzed by Auger electron spectroscopy (AES) using a Physical Electronics Industries PHI 10-234GC spectrometer. Thick coatings of the powders were pressed into Al substrates and 3 keV, 30 μA normal incidence electron beam was used as the excitation source (cylindrical mirror analyzes with co-axial gun). Spectra were recorded at a baseline pressure of 5×10^{-10} Torr for untreated samples, and in 5×10^{-5} Torr argon after argon ion bombardment. The electron and ion beam current were measured using a Keithly 610B electrometer.

The spectrometer was equipped with the PHI 20-055 multiplex control so that measurement of the peak-to-peak height at 6 different electron energies could be carried out concurrently with ion bombardment.

X-Ray photoemission spectroscopy (XPS) was used to distinguish the chemical states of W, C, and O on the carbide surfaces. A McPherson ESCA 36 spectrometer was used with the samples mounted in exactly the same manner as for AES.

c. *Preparation of Electrodes*

The carbide powders were fabricated into porous, PTFE-bonded, hydrophobic electrodes using a procedure described previously (*16*a) with some modifications. Wet-proofed carbon paper was used as the substrate, and the PTFE content in the catalyst layer varied from 5 to 50 w/o. The catalytic activities of the WC catalysts for the electrochemical oxidation of H_2 were measured using the half-cell design of Vogel and Lundquist (*16*b). The electrodes were placed in the cell under H_2 purging and filled with electrolyte by standing at the H_2 open circuit for 24–72 hr. For activity measurements in H_3PO_4 at 120–180°C, 85 w/o ortho-phosphoric acid, purified by chromic acid treatment, was concentrated to 85–100 w/o, the concentration increasing with increasing temperature. H_2 for both the reference and working electrodes was saturated with H_2O at 25–60°C. The reference electrode was Pt black, the counter electrode was a graphite rod. The current–potential characteristics were recorded galvanostatically, with the electrode potential corrected for the ohmic resistance of the electrolyte by the current-interruption method (*17*). No hysteresis was observed in the I–V characteristics. The performance of some of the electrodes

TABLE 1

Tungsten Carbides Prepared by Carburizing Tungstic Acid Hydrate

Sample No.	Modification of tungstic acid	Carburization condition		Carbon content (w/o)	Surface area (m^2/g)
		Temp (°C)	Time (hr)		
7P	Yellow	700	4	6.2	15
22P	Yellow + 10 w/o NH_4Cl	700	4	6.0	15
41P-1	White (crystalline)	900	2	6.1	5
41P-2	White (crystalline) + 10 w/o NH_4Cl	900	2	6.1	5
70P	White (amorphous)	700	4	5.8	15
84P	White (amorphous) + 10 w/o NH_4Cl	700	4	5.5	17
165	White (amorphous) + 10 w/o NH_4Cl	900	2	5.1	8
AEG	Not available	Not available		5.8	5

was improved after several load cycles in which the potential varied from 0–0.35 V (RHE). The steady state I–V characteristic was taken after no further changes in performance took place.

RESULTS

a. Characterization of the Bulk Properties

An index of the different preparations of the unsupported carbides and the resulting bulk composition and surface areas are given in Table 1. The X-ray diffraction characteristics of these powders are given in Fig. 1, along with the spectra for the pure phases WC and α-W_2C (*18*). There were significant differences in the crystal structure of the tungsten carbide depending on whether the yellow or white modification of the tungsten acid hydrate was used. Carburization of the yellow form yielded essentially the ideal carbide lattice (comparing Fig. 1-1 and 1-6). and of the white forms yielded a distorted lattice with the [110], [002], [003], [202] reflections diffuse. The distorted lattice appeared to be correlated with a carbon lattice deficiency in the bulk stoichiometry, as Table 1 indicates, and this carbon deficiency was apparently enhanced by the addition of NH_4Cl to the tungstic acid hydrate.

The supported WC and W_2C catalysts produced X-ray diffraction patterns identical to that of the pure material. The transmission electron micrographs of the two materials are shown in Fig. 2, from which the average crystallite size ($\bar{d}_v$) was calculated to be 275 and 385 Å, respectively. For the purposes of normalizing the kinetic parameters for these catalysts, a surface area was calculated as $S = 6/(\rho \bar{d}_v)$.

b. Electrocatalytic Activity for H_2 Oxidation in Acid

A series of experiments was conducted to determine diffusion effects in the electrodes fabricated from the tungsten carbide powders. Diffusion effects in electrodes with the "layer" geometry have been analyzed previously (*19–22*). The "liquid film" gas diffusion limiting current (*20*) is more than an order of magnitude greater than the current densities measured here, and ionic diffusion in the electrolyte is rapid compared to diffusion of dissolved gas (*22*).

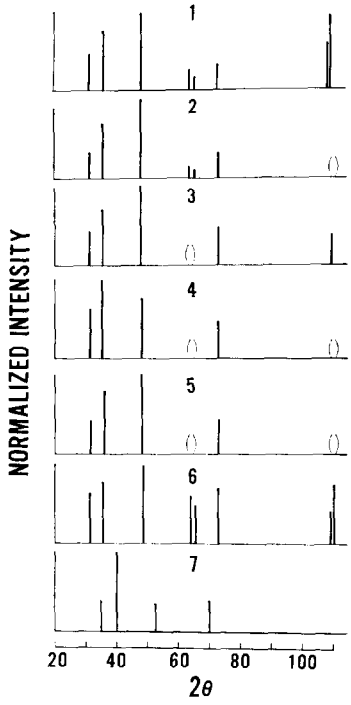

FIG. 1. X-Ray diffraction (Cu$K\alpha$) spectra of different preparations of high surface area WC. Intensity normalized by the most intense reflection in each sample. (1) 7P; (2) 22P; (3) 41P; (4) 70P; (5) 84P; (6) ASTM standard for α-WC; (7) ASTM standard for α-W_2C.

For electrodes in which gas diffusion effects are absent, the current density at fixed electrode potential (η) should increase linearly with catalyst loading, and at sufficiently high loading approach the loading-independent region of mixed diffusion and activation control. The activation energy $R(\partial \ln i/\partial 1/T)_\eta$, in the region of mixed control is one-half the activation energy in the loading-dependent, kinetically controlled region. Figure 3a shows the optimization of the PTFE content for a WC powder with a BET surface area of 8 m^2/g, and Figure 3b shows the corresponding loading dependence of the current density for electrodes containing the optimum PTFE content. For PTFE contents less than the optimum the activation energy was 4 kcal/mole rather than 8 kcal/mole as at the optimum, indicating diffusion effects are predominant. Greater than 30 w/o PTFE resulted in incompletely wetted catalyst (confirmed independently by double-layer capacity measurements). Electrodes containing less than 15 mg/cm^2 tungsten carbide with 30 w/o PTFE therefore appeared to be free of gas diffusion effects and differences in current–potential characteristics of the electrodes could be attributed directly to differences in catalytic properties.

The steady-state current–potential characteristics of some of the carbide powders are shown in Fig. 4. A complete tabulation of the activity levels of the various preparations of the carbides is given in Table 2. Results obtained using a tungsten carbide powder supplied by Dr. H. Boehm of AEG-Telefunken are also included in Tables 1 and 2 (labeled AEG) for comparison. This powder had been used in the previous studies of Levy and Boudart (*13*) and Ross *et al.* (*14, 15*). The current densities have been normalized by the BET surface area of the powder. The activation energy for H_2 oxidation, defined as $-R(\partial \ln i/\partial 1/T)_\eta$, was the same for all the carbides tested (8 kcal/mole). Some activity measurements were also carried out at much lower temperatures in H_2SO_4 for purposes of comparison with previously reported activities for WC. Figure 5 shows an Arrhenius plot for the activity of tungsten carbide with the ideal structure synthesized by fusion of the elements, and shows that (a) the activity is the same in H_3PO_4 as in H_2SO_4; (b) the activity level is the same (within factor of 2) as that reported by others (*23–25*) for stoichiometric WC using nonporous (hot pressed or highly sintered) electrodes. The stability of the various preparations towards polarization greater than 0.35 V varied considerably. Preparations 7P, 22P, 39P1, and 75P all suffered irreversible activity loss at potentials anodic of 0.35 V (RHE), whereas all other preparations were either unaffected or improved slightly. None of the tungsten carbide

electrodes was poisoned by any carbon monoxide present in the H_2, i.e., performance levels on CO/H_2 mixtures were identical to N_2/H_2 mixtures.

c. *Activation of Tungsten Carbide by Mild Oxidation*

Selected preparations were exposed to a mild gas-phase oxidation treatment. Such a treatment has been claimed in a German patent (*12*) as enhancing the activity of tungsten carbide, with the optimum "activation" produced by flowing O_2 over the catalyst for 30 min at 350°C. The response of samples 7P and 70P to oxidation in flowing O_2 at 350°C is shown in Fig. 6. The results of 30 min oxidation treatment on the other samples is shown in Table 2. Only tungsten carbide prepared via the white modification of tungstic acid hydrate responded positively to this "activation" treatment. Carbide prepared by carburization of the yellow modification of tungstic acid or by fusion of the elements was adversely affected by this oxidation treatment. Ditungsten carbide (W_2C) prepared by fusion of the elements was completely deactivated by the oxidation treatment.

TABLE 2

Catalytic Activity of Various Preparations of Tungsten Carbide

Sample No.	Specific current density @0.05 V (RHE), mA/m²	
	Initial	After gas-phase activation
7P	16	—
22P	18	9
41P-1	145	—
41P-2	140	—
70P	56	115
84P	255	No change
165	220	No change
AEG	370	—
39P1	105	25
75P (W_2C)	26	Polarized

d. *Characterization of the Carbide Surface by AES and XPS*

AES was used to obtain a quantitative measure of the surface composition of the carbide powders in order to relate (i) the surface composition to the method of preparation; (ii) changes in surface composition to the activation treatment. XPS was used to distinguish different chemical states of the tungsten, carbon and oxygen atoms in the surface layers.

All Auger spectra were recorded in the derivative mode. In the derivative spectrum, the relative concentration of an element is proportional to the peak-to-peak height at the energy of a single Auger transition. Calculation of the surface composition followed the method of Palmberg *et al.* (*26*) and was based on sensitivity factors determined for the pure elements. The Auger transitions selected for composition analysis were: for carbon, the *KLL* transition at 270 eV; for oxygen, the *KLL* transition at 505 eV; for W, the $N_5N_6N_{6,7}$ [assignment of Chung and Jenkins (*27*)] at 163 eV. The analysis of the surface composition was complicated by the contamination of all the samples on exposure to air, and significant changes in lineshapes of the family of Auger transitions at 240–275 eV. Figure 7 shows the Auger spectra for the outer surface of a nonporous tungsten carbide (WC) rod, the *in vacuo* cleaved surface, and the depth-profiling (simultaneous ion sputtering and spectroscopic analysis) of the outer surface. Ion sputtering revealed a very thin layer, less than a monolayer, of carbon in excess of the bulk stoichiometry due to exposure of the rod to air. That the excess carbon was most probably due to contamination was indicated by the observation of similar carbon levels on pure metals such as Pt, Rh, and Au. There is a significant difference in the fine structure of the carbon *KLL* Auger transition between carbon in graphite and carbon in the metal carbides. This was

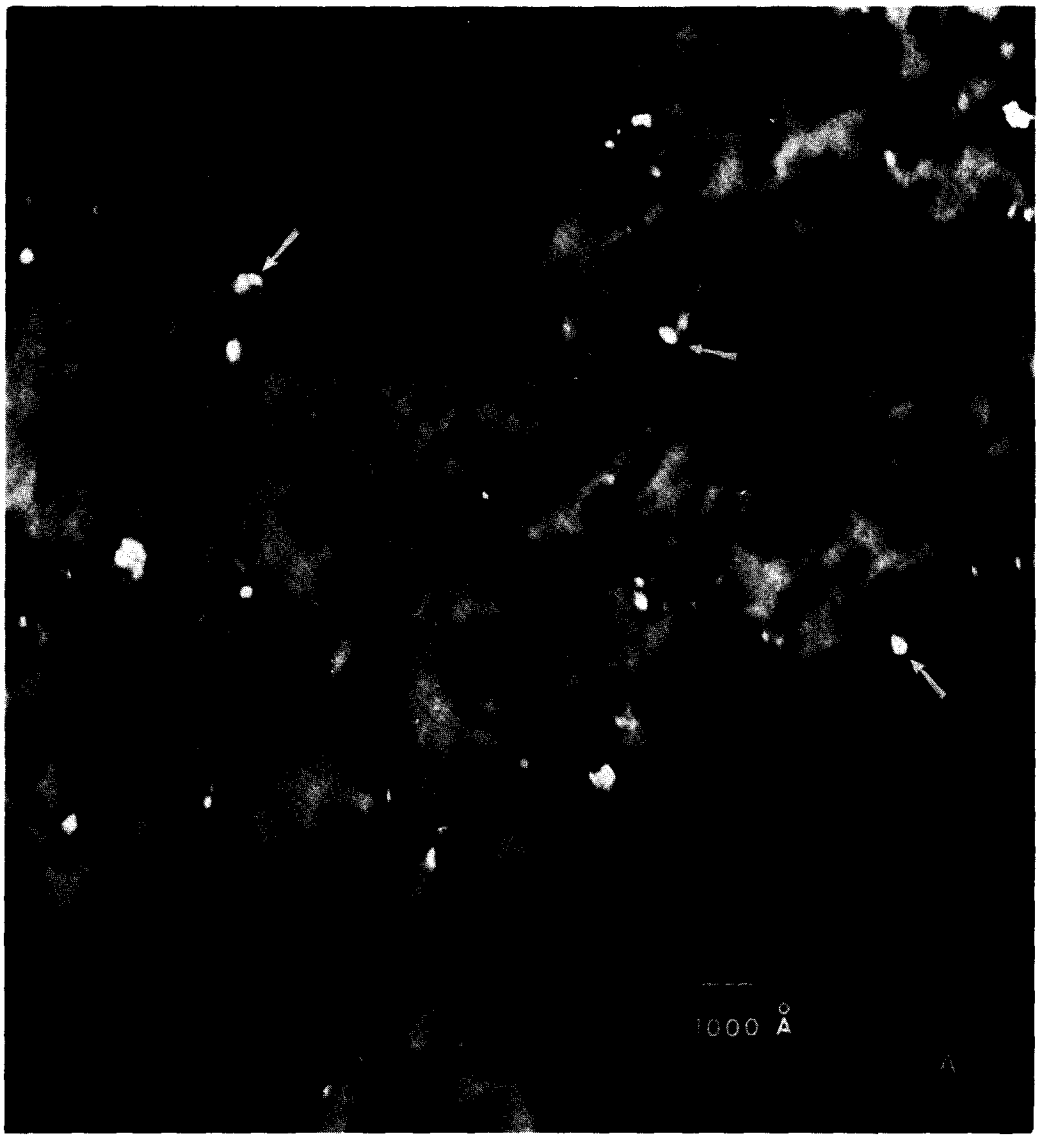

FIG. 2. Transmission electron micrographs of WC and W_2C crystallites on a carbon black support: (A) dark field of WC (sample 39P1); (B) W_2C (sample 75P).

observed previously by several investigators (*28–30*). This difference in fine structure may be used to determine the presence of free carbon (i.e., noncarbide) on the surface of tungsten carbide. No significant differences could be observed in the fine structure of the carbon *KLL* transitions of WC and W_2C cleaved *in vacuo*. The relative sensitivity factors determine for the pure elements resulted in a calculated composition for these cleaved surfaces identical (±3 a/o) to the known stoichiometry. Figure 7 also shows that extensive low energy ion sputtering (0.5–1 keV, 85 μA) did not alter the W/C ratio in the pure WC phase.

The calculated surface compositions of the untreated catalysts, shown in Table 3, indicated a large difference in surface carbon content between the most cata-

FIGURE 2B

lytically active samples, 84P, 165, AEG, and the least active samples, 7P and 70P. That the large excess of surface carbon was in the form of free carbon was evidenced by the differences in fine structure of the carbon *KLL* transitions (Fig. 8). The free carbon was rapidly ion sputtered from the surface, with the ion sputtering stopped when the relative intensities of the carbon *KLL* transitions at 250, 258, and 268 equaled those for the clean, stoichiometric WC surface (Fig. 8d). Since the samples were porous powders, it was not possible to estimate the depth of the excess layer from the sputtering rate of carbon determined using thin film techniques (*31*). If it is assumed that the free carbon covers a surface having the stoichiometry of the bulk carbide, then the carbon thickness can be estimated from the ratio of the intensi-

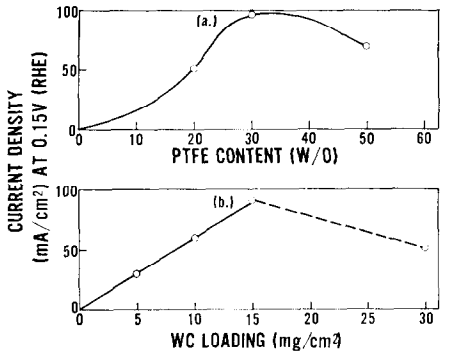

FIG. 3. Variation of performance of a PTFE-bonded high surface area (8 m^2/g) WC electrode. Current density at 0.15 V (RHE) as a function of (a) PTFE content, fixed loading of 15 mg/cm^2; (b) WC loading, fixed PTFE content of 30 w/o.

ties of the W 164 eV Auger electrons before (I) and after (I_0) removal using the analysis of Seah (*32*),

$$x_c = 0.74\mu_{160}{}^c \log_e(I_0/I)$$

where $\mu_{160}{}^c$ is the attenuation length of an 160 eV electron in carbon. Using an attenuation length of 6 Å (*33*), the free carbon layer on samples 7P and 70P is estimated to be 7.5 Å, or approximately 2–3 monolayers. There was a slight excess of carbon relative to the bulk stoichiometry on even the most catalytically active preparations, 84P, 165 and AEG. We feel this slight excess is contamination of the samples by prolonged exposure to air, resulting in weakly adsorbed carbonaceous species, and by the process of pressing the powders into the Al substrates for mounting in the spectrometer.

Activation of preparations 7P and 70P produced similar changes in the surface composition, with the W/C ratio being substantially increased in both, but the oxygen level much higher in the case of 7P. Depth-profiling (Fig. 9) revealed substantial differences in the atomic distribution of the surface layers. In 70P, the outermost surface is slightly carbon deficient (C/W < 1) with a thin oxygen layer covering *both* tungsten and carbon atoms. In 7P, oxygen has penetrated much deeper into the surface, with the outermost layers still containing an excess of carbon (C/W > 1). The fine structure of the carbon *KLL* transitions of 7P-activated showed evidence of free carbon, whereas 70P-activated did not. The oxidation at the surface of these two carbon covered carbides is clearly different. In the case of the bulk stoichiometric carbide, oxidation into the bulk takes place simultaneously with oxidation of the free carbon. In the carbon deficient carbide, oxidation of free carbon and only the outermost surface layer occurs.

XPS was used to examine possible differences in the chemical states of the surface atoms in the different preparations. The carbon 1*s* binding energy (BE) in WC is shifted from the BE in graphite by −1.8 eV, the W 4*f* BE in WC is shifted −0.3 eV relative to W metal, and in WO_3 (W^{6+}) is shifted to +4.5 eV relative to tungsten metal (*34*). These chemical shifts make it possible to distinguish, in principle, free

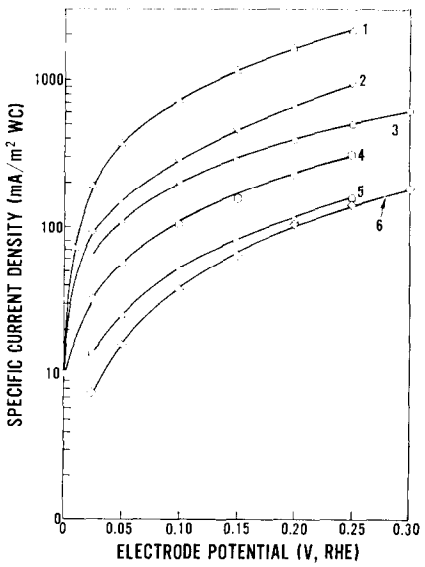

FIG. 4. Hydrogen oxidation polarization curves for preparations of high surface area tungsten carbides: (1) AEG; (2) 41P1; (3) 39P1; (4) 70P; (5) 7P; (6) 75P (W_2C). 98 w/o H_3PO_4; 177°C; 1 atm H_2.

carbon from carbide carbon, oxidized tungsten from carbide tungsten from free tungsten (metal). In practice, the relative ratio of free carbon to carbide carbon could not be made with certainty due to a problem of carbon contamination on the sample *inside* the McPherson spectrometer. Even after pumping the sample chamber to UHV conditions of 5×10^{-10} Torr, a sample cleaned by ion bombardment quickly became contaminated with carbon although this contamination could be reduced by use of very short counting times (10 min). The carbon 1*s* spectra nevertheless showed the same relative distributions of free carbon to carbide carbon as was observed in the *KLL* Auger spectra. Comparison of spectra for 70P with 84P (Fig. 10b and c) show a much larger total surface concentration for carbon in 70P, most of this excess being free (noncarbide) carbon. Nearly all the free carbon on 84P was contamination from the vacuum system of the McPherson spectrometer, as concluded by a comparison of the height of the 284.3 eV peak in 84P with the carbon contamination peak on a WO_3 powder sample (Fig. 10a). Carbon 1*s* spectra for 7P were nearly identical to that for 70P, and the 84P, 165 and AEG spectra were all practically identical. The W 4*f* spectra indicated that major differences existed in the chemical state of the surface W atoms in the different carbide preparations. The spectra of the most active carbides (84P, 165, AEG) all indicated a significant fraction (30–40%) of the tungsten atoms were in the +6 valence state after preparation and prolonged exposure to air, while the least active (7P, 70P) forms contain essentially no W^{6+}, as shown by the spectra in Fig. 11. Tungsten carbide (WC) prepared by fusion of the elements in an inert atmosphere, and removal from the furnace *cold*, did oxidize in air at room temperature to form 10–20% W^{6+}. W_2C formed a much larger amount of W^{6+} than WC (Fig. 11c). Following the oxidation activation treatment of 7P and 70P, nearly all the free carbon was removed from the surface, with 25% of the W atoms converted to W^{6+}, in each case. The oxidative activation treatment had no discernible effect on the spectra of 84P, 165, or AEG, but WC prepared by fusion of the elements was converted to more than 50% W^{6+}.

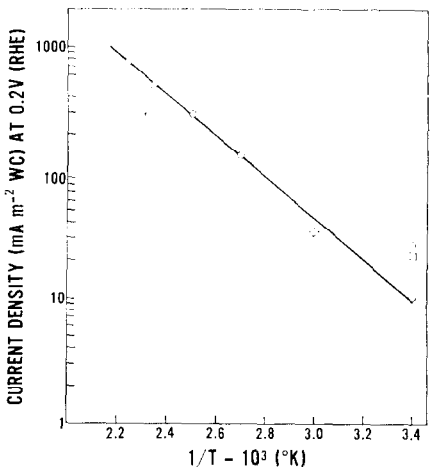

FIG. 5. Arrhennius plot of catalytic activity (1 atm H_2) of stoichiometric (39P1) WC for data of this study for concentrated H_3PO_4 (○), for H_2SO_4 (▽) compared to previously reported results in H_2SO_4: (◇) Barasel *et al.* (*24*), (○) Mund *et al.* (*4*), (□) Sokolsky *et al.* (*25*).

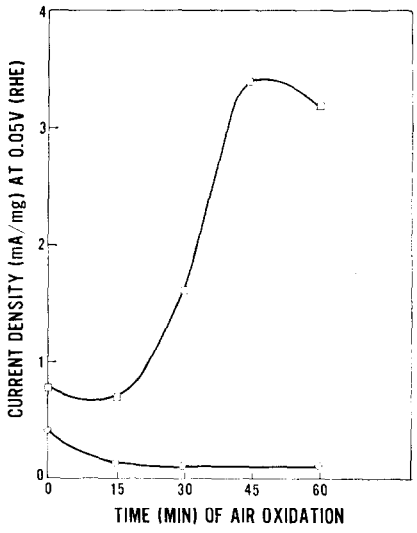

FIG. 6. Effect of oxidative activation of WC preparations (□) 7P and (○) 70P on electrode performance. 98 w/o H_3PO_4; 182°C; 1 atm H_2.

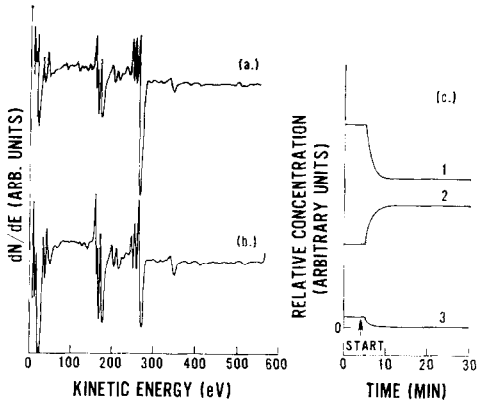

FIG. 7. Auger electron spectra of (a) external surface of a nonporous tungsten carbide (WC) rod; (b) the *in vacuo* cleaved surface; (c) external surface exposed by ion sputtering: (1) C, (2) W, (3) O. 2 V (p–p), lock-in amplifier time constant OFF. Ion beam at 1 keV, 85 μA.

DISCUSSION

The fine structure in the carbon KLL Auger transition spectra of "clean" tungsten carbide is related directly to the nature of the metal–carbon bonding in the refractory metal carbides. A model system for bonding in these carbides is TiC for which reliable band calculations have been made (*35*) and used by Ramquist (*36*) to interpret the X-ray absorption and photoemission data.

The valence band photoemission spectra of TiC showed a core-like state 11 eV below the Fermi level (E_F) superimposed on the tail of the valence band centered 3 eV below E_F. Using the band calculations Ramquist assigned these levels to the C2s and C2p–Ti3d states with the latter closest to the Fermi level. This assignment of levels indicates there is little or no sp hydridization of the carbon atom in TiC. If these two electronic states are denoted V_1 and V_2, respectively, using the K level of carbon in TiC (*36*) at (E_F − 281.8) the Auger transitions KV_1V_1, KV_1V_2, KV_2V_2 would be expected at approximately 260, 268, and 275 eV (uncorrected for work function). Experimentally, the fine structure of the carbon Auger transition in TiC (*30*) indicated transitions at 270, 262, and 254 eV, in close agreement with the expected values for a work function of ~5 eV. Although the metal–carbon bonding in WC has not been established with the same certainty as in TiC, the photoemission spectra of WC (*34, 37*) indicates the W–C bonding is qualitatively similar to the Ti–C bonding. The C2s state occurs as a core-like state 12 eV below E_F, with the C2p–W5d band centered at (E_F − 3) eV. Using the K level observed for carbon in WC (Fig. 10) the expected Auger transitions would then occur at 259, 268, and 277 eV, which agrees with the relative positions of peaks in the observed spectra (Fig. 8). The fine structure at 270–272 eV observed in WC Auger spectra (and not in TiC) probably reflects the structure seen in the p–d band at 1.8 and 3.4 eV below E_F (*37*). The two sharp Auger transitions observed between 245–270 eV for TiC and WC are not observed in graphite or carbon black. Hydridization of the carbon 2s and 2p levels to form the sp bonding orbitals characteristic in these materials results in a broad (25 eV) flat band and an Auger

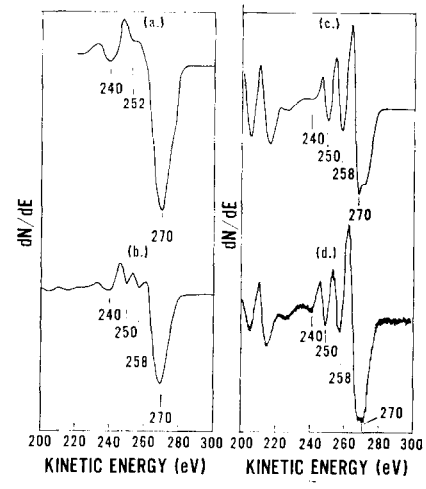

FIG. 8. Fine structure of carbon KLL Auger electron spectra in (a) stress-annealed graphite; (b) 7P; (c) 84P; (d) *in vacuo* cleaved WC rod. 2 V (p–p), lock-in amplifier time constant 10 ms.

spectra with no fine structure between 245–270 eV. The broad peak in the Auger spectra of graphite at 240 eV was identified by Coad and Rivere (*29*) as a plasmon loss suffered by 270 eV electrons. Recent electron energy loss measurements for graphite (*38*) support this assignment. Thus, the use of the fine structure of the carbon Auger spectra to differentiate the chemical state of carbon in the carbide preparations derives from current knowledge of the metal–carbon bonding.

The rate at which hydrogen is being consumed electrochemically, v, is directly proportional to the current density, i, by the relation

$$v = (N/S)\cdot(i/nF) \equiv \text{molecules/surface atom-sec}, \quad (1)$$

where n is the number of electrons transferred per equivalent, F is the Faraday constant, N is Avagadro's number, S is the number of surface atoms per unit area of catalyst, and i is the current per unit area of catalyst in the electrode (mA/m²). The quantity v, which is an equivalent to the turnover number used in gas-phase catalysis, is a function of electrode potential with the general form,

$$v = K\cdot\varphi(E - E_0),$$

where K is a chemical kinetic term, E_0 is the equilibrium potential for the half-cell reaction (in this case zero) and $\varphi(E - E_0)$ is a function representing the electrochemical driving force. The exact form of these functions will depend on the mecha-

TABLE 3

Surface Composition of High Surface Area Tungsten Carbides

Preparation	Surface composition (a/o)					
	Initial			After ion-bombardment[a]		
	W	C	O	W	C	O
7P	17	82	1	47	53	—
7P following activation	36	45	11	52	44	4
70P	14	85	1	49	51	—
70P following activation	33	58	7	48	51	1
84P	42	50	7	45	44	10
165	41	50	8	45	40	15
AEG	41	45	14	55	38	7

[a] See text for ion-bombardment duration.

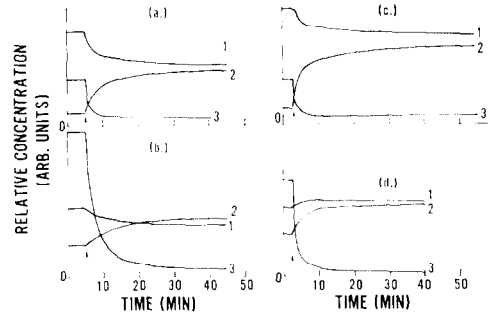

FIG. 9. Relative surface concentrations of preparations (a) 7P; (b) 7P "activated"; (c) 70P; and (d) 70P "activated"; as a function of sputtering time: (1) C, (2) W, (3) O. Ion beam at 1 keV, 85 μA.

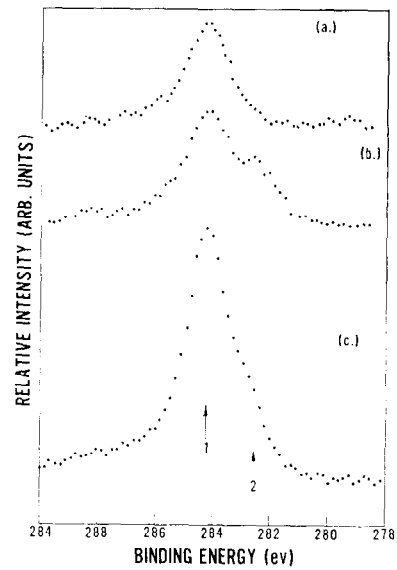

FIG. 10. X-Ray photoemission spectra from C (1*s*) for (a) WO_3; (b) WC preparation 84P; (c) WC preparation 70P. (1) Position of C (1*s*) in graphite, (2) in WC. Binding energy is referenced to C (1*s*) contamination line at 284.3 eV.

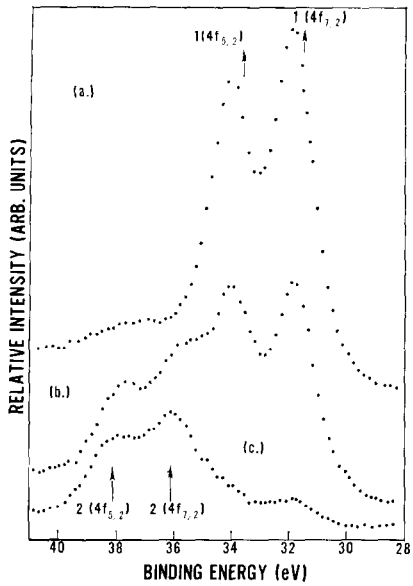

FIG. 11. X-Ray photoemission spectra from W(4*f*) levels for WC preparations (a) 7P; (b) 84P and for (c) pure W_2C prepared by fusion of the elements. (1) Position of W(4*f*) level in oxide-free tungsten metal; (2) in WO_3. Binding energy is referenced to C(1*s*) contamination line at 284.3 eV.

nism for the reaction. In electrocatalysis, we are interested in isolating the chemical kinetic term since this term reflects the catalytic factor in the reaction rate. A qualitative comparison of catalytic activity of different catalysts can be obtained by comparing i (or v) at a fixed potential E, but the comparison will always contain some effect of $\varphi(E)$ if the mechanism differs between catalysts. This effect can be minimized by choosing $(E - E_0)$ to be as small as practical. For the hydrogen reaction on reasonably active catalysts, we have found 0.05 V (RHE) to be an appropriate potential, and we have chosen to compare the levels of catalytic activity of different preparations of tungsten carbide by using the specific current density at 0.05 V (RHE). The rate of hydrogen consumption at 0.05 V (RHE) can easily be computed from the specific current density and Eq. (1). As an example of this, the most active tungsten carbide catalyst exhibited a specific current density of 370 mA/m^2 corresponding to a hydrogen consumption rate (turnover number) of 0.093 (molecules/surface atom-sec). The specific current densities that are tabulated in Table 3, therefore, are a quantitative measure of the relative catalytic activity of the different tungsten carbide preparations.

The electrocatalytic activities of the freshly prepared catalysts whose surface compositions by AES were approximately stoichiometric exceeded that of catalysts whose surfaces contained an excess of carbon (free) by more than an order of magnitude. It is clear that some WC preparation conditions result in the deposition of free carbon on the surface of the carbide, the free carbon being inactive for H_2 oxidation. On the basis of electrochemical charging curves Palanker *et al.* (*39*) postulated that carburization of tungsten by CO at 700–800°C resulted in a deposit of carbon black on the tungsten carbide surface, whereas carburization at 1000°C yielded a clean stoichiometric surface. In a previous study (*15*), we showed by AES that this hypothesis is correct for the carburization of CO at tungsten metal pre-reduced in H_2. The results of the present study clearly show that carburization of tungstic acid hydrate by CO at 700°C also leads to the deposition of free carbon on the carbide surface, but at 900°C this deposition is much less (comparing samples 7P to 41P-1). The addition of 10 w/o NH_4Cl to the tungstic acid hydrate appeared to inhibit this deposition almost entirely (70P vs 84P). One explanation of this effect both of temperature and NH_4Cl on the carbon formation problem is depicted in Fig. 12. The principle chemical reactions taking place in carburization are reduction of WO_3 to W by CO or carbon, deposition of carbon by catalytic decomposition of CO, and dissolution of carbon into W. Figure 12 depicts the events at an intermediate stage of carburization of a WO_3

crystallite (on the order of a 100–300 Å) with a WC outer surface and a WO_3 core. CO is decomposed to carbon catalytically at WC or W but not at the free carbon surface, carbon and oxygen counter-diffuse through the WC mantle, the carbon reacting with tungsten metal, the oxygen reacting at the free carbon boundary or with gas phase CO to form CO_2. The ratio of clean WC surface $(1 - \theta)$ to carbon covered (θ) WC surface will, therefore, be proportional to the ratio of the diffusivity of carbon in WC to the rate constant for carbon deposition. Since the temperature coefficient (E_D) for carbon diffusion through the carbide phase [e.g., Williams (*40*) reported $E_D > 90$ kcal/mole for C in TiC, TaC, NbC] is much larger than the activation energy (*41*) for catalytic dissociation of CO [20 kcal/mole on Fe], the ratio of the clean to carbon covered surface will increase with increasing temperature. The effect of NH_4Cl may be explained in terms of this model if it is assumed that chlorine released when the NH_4Cl decomposes adsorbs strongly on the surface of the tungstic acid crystallite and remains adsorbed on the outer surface of the crystallite during carburization. The adsorbed Cl^- might be expected to poison the CO disproportionation reaction, similar to the effect chlorine treatment has for carbon deposition on aluminas. This would lower the ratio of D/k_c, and, therefore, the ratio of clean to carbon covered WC surfaces.

One of the effects of the gas-phase activation treatment was to remove the surface excess free carbon via oxidation to CO_2. This was reflected directly by both the AES and XPS results. It seems likely that the electrochemical activation (*23*) treatment of WC by anodic 1 V pulses has a corresponding effect of oxidation of any free surface carbon. The XPS spectra showed that the oxidation process does not necessarily stop when the surface free carbon is removed, but continues to remove carbon from the carbide and oxidize the

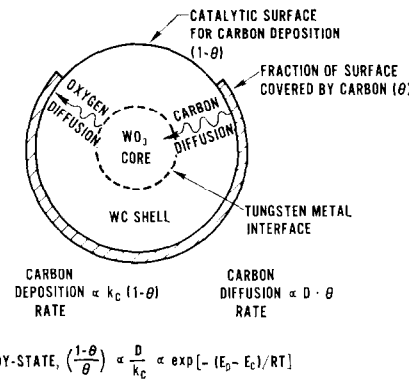

FIG. 12. Idealized model for the carburization of tungstic acid (or WO_3) by carbon monoxide.

tungsten atoms to W^{6+}. The stability of the clean or oxidatively cleaned carbide surface towards further oxidation depended on the bulk stoichiometry of the carbide. Depth-profiling by AES indicated that prolonged exposure of the bulk stoichiometric monocarbides (7P, 41P, 39P) to O_2 at 350°C produced oxidation of the bulk structure and nearly complete oxidation of the surface to WO_3. In the case of the bulk carbon deficient carbide (70P), exposure to O_2 at 350°C produces an equilibrium surface that is a mixture of a tungsten oxide (25 a/o W^{6+}) and tungsten carbide (75 a/o W^0). In the case of the carbide preparations 84P, 165, AEG, this equilibrium is apparently already present as the oxidation treatment had little effect on either the AES or XPS spectra or on catalytic activity. AES indicated a significant amount of oxygen is present both at the surface and in the bulk of these latter preparations. It is well known that transition-metal carbides, particularly the Group IV–VI metal carbides, can dissolve considerable oxygen by substitution for carbon (*42*). Comparison of the ionic radius of oxygen anions (1.45 Å) and the covalent radius of the oxygen atom (0.66 Å) with the covalent radius of carbon in WC (0.77 Å) indicates that oxygen substituted for carbon in WC is in a covalent bonding state. Dissolution of oxygen into the carbide

lowers the activity of both the metal and carbon atom and reduces the oxidation rate of the carbide. It seems probable that the carbon vacancies of preparations 84P, 165, and AEG are filled by oxygen, and that the presence of this lattice oxygen stabilizes the surrounding carbide lattice towards oxidation to WO_3 and CO_2. A more definitive picture of the crystallography of these oxygen rich, carbon deficient carbides could be obtained by an analysis of the X-ray intensity profiles in Fig. 1, but this analysis was beyond the scope of the present investigation. Even in the absence of a definitive analysis, the known chemistry of the Group VI metal carbides and the direct observation by AES of the relative amounts of W, C, and O indicate oxygen dissolution by substitution for carbon in the preparations.

The dissolution of oxygen into the carbide was clearly dependent on the preparation method. Only when the white modification of tungstic acid hydrate was used as a starting material did significant oxygen substitution occur, and this was optimized by using the high surface area amorphous form combined physically with NH_4Cl. Svata and Zabransky (*8, 9*) had reported the same observation and attributed the resulting carbide structure to the defect structure of the white modification. The defect structure was postulated as creating a defect tungsten structure on reduction that is reflected in the carbide structure. The X-ray diffraction patterns of the carbon deficient preparations do show distortion along selected crystallographic planes, principally the [002] and [110] planes. The [002] plane is the plane containing only carbon atoms, the [110] plane contains W and C atoms in a 2:1 ratio. The major crystallographic planes containing primarily W atoms (e.g., [001], [100], [101], [111]) showed no change in position or intensity. The lattices of the carbon deficient carbides do appear to have distorted carbon positions, due either to carbon vacancies or to oxygen substitution. How the carbide structure is related to the defect structure of the tungstic acid is unclear. Oxygen substitution in the transition metal carbides occurs readily when the lattice is not fully saturated with carbon (*42*). Boehm and Pohl (*6*) found that carburization of W metal by CO proceeded via W_2C as an intermediate state. One might expect, therefore, in terms of the carburization model of Fig. 12, at the boundary between the WO_3 core and the WC shell there is an intermediate state like W_2C where oxygen substitution from WO_3 may occur. Why this substitution is specific to a particular modification of tungstic acid and enhanced by NH_4Cl has not been determined. The electrocatalytic activity of a carbon covered bulk substoichiometric carbide (70P) following gas-phase activation was much greater than that of the bulk stoichiometric carbide (7P) following gas-phase activation. XPS indicated that both preparations after activation had a similar fraction of the surface as an oxide ($\sim$25% W^{6+}). The activation of tungsten carbide preparations by gas-phase oxidation can remove the free carbon from the carbide surface, but probably does not substitute oxygen for carbon in the carbide lattice.

The catalytic activity per BET unit area for electrochemical oxidation of hydrogen in acid of the carbon deficient, oxygen-containing carbides was observed to be significantly (about a factor of 3) greater than the activity of the stoichiometric (both surface and bulk) carbide. Svata and Zabransky (*8*) used preparation procedures that according to our work would have produced the stoichiometric WC and the carbon deficient carbide and reported a factor of 2 difference in activity between these preparations. There are numerous reports in the electrochemical literature of an enhancement in the hydrogen activity of WC prepared by fusion of the elements (thus a clean and not carbon covered surface) produced by anodization, usually

TABLE 4

Relative Electrocatalytic Activity for H_2 Oxidation in Acid at 25°C

Catalyst	Pt	Rh	Ru	WC	Au	Carbon
Activity	1	0.5	7×10^{-2}	10^{-4}	5×10^{-5}	$<10^{-6}$
Ref.	(*44*)	(*44*)	(*47*)	This work	(*48*)	(*48*)

in the presence of a reducing agent in the electrolyte, e.g., H_2 or hydrazine (*10, 11*). Thus, while the differences in activity are not large in an absolute sense, they have been observed repeatedly by numerous experimenters and there can be little doubt that they are real and significant. This conclusion leads naturally to the consideration of the true nature of the active surface or the active sites of the tungsten carbide surface for hydrogen chemisorption and oxidation. The *active* surface contains oxygen atoms in addition to tungsten and carbon. The oxygen atoms are in two different chemical bonding states, a covalent state and an anionic (O^{2-}) state. The tungsten atoms are also in two valence states, W^{6+} and W^0, the latter with some degree of positive charge (*36*). The O^{2-} anions are probably associated with the W^{6+} ions and corresponds to some portion of the surface present as WO_3 clusters. The zero valent state of tungsten represents covalent bonding of tungsten to carbon and oxygen atoms. We propose that the bonding of tungsten to the oxygen in the carbon lattice positions is very similar to the W–C bonding, i.e., primarily W5*d*–O2*p* with some (0.3*e*) charge transfer from tungsten to oxygen. In electrolyte solution at hydrogen anode potentials, 0–0.1 V (RHE), surface W^{6+} is reduced to the equilibrium W^{5+} oxidation state (*43*), but this surface does not chemisorb hydrogen and is a poor catalyst for the hydrogen electrode reaction. The stoichiometric WC surface is stable in acid electrolyte at anodic potentials of 0–0.3 V, but at greater than +0.3 V severe oxidation takes place (*10*). The catalytically active carbon deficient carbide surface is, however, stable to more anodic potentials (to +0.6 V) but pure W_2C is much less stable towards oxidation than even stoichiometric WC. The oxygen substitution for carbon with the W–O covalent bond, and not the carbon deficiency itself, produced the stabilization of the carbide surface. This observation follows a general trend of the transition metal carbides that the oxycarbide is often a more useful material under oxidizing conditions that the pure carbide (*42*). In the absence of electrolyte, i.e., in the gas-phase, tungsten metal is one of the most active metals for hydrogen dissociation, at least as active as Pt (*44*). Since hydrogen dissociation is the rate determining step in the electrochemical oxidation of hydrogen on Pt in acid, one would suspect that in the absence of interference from the electrolyte surface tungsten atoms in the "metallic" (zero valent) state would be sites for hydrogen dissociation. From the electrochemical corrosion behavior of WC compared to tungsten metal, it is apparent that W–C bonding stabilizes the tungsten atoms towards oxidation by the acid electrolyte and produces a surface containing a significant concentration of "metallic" tungsten atoms. According to Sturms (*42*), and as the electrochemical behavior of the oxygen substituted carbide indicated, oxygen substitution for carbon stabilizes both the tungsten and carbon atoms and lowers the activity of each towards oxidation. Since the oxidation of WC in acid proceeds via the attack of H_2O molecules from the electrolyte (*45*), W–O covalent bonding probably reduces the interaction of H_2O with the surface O–W–C site. The adsorbed

H_2 molecules can now compete more effectively with H_2O for the active "metallic" site, and the rate of H_2 oxidation might, therefore, be expected to be faster at the O–W–C sites than the C–W–C sites.

Comparison of Active WC with other Electrocatalysts

It is of both practical and fundamental interest to compare the catalytic activity of the most active form of tungsten carbide to that of other materials. Table 4 lists the catalytic activities for hydrogen molecule oxidation in acids at 25°C for several materials relative to that for Pt. The activity levels are valid only for small (<50 mV) anodic overvoltages. The reference absolute activity level for Pt is an exchange current density of 3×10^{-2} A/cm^2 (*44*), corresponding to a turnover number for H_2 consumption *at equilibrium* of 75 (molecules/surface atom-sec). The most active forms of WC are more active than Au or any of the metals which do not chemisorb hydrogen, e.g., Cu, Ag, Al, Hg, etc. [see Trasatti (*46*)], but is significantly less active than the Pt group metals, e.g., Pt, Ir, Pd, Rh, and Ru. This grouping of activity levels suggests that either tungsten carbide does not catalyze H_2 oxidation via dissociative chemisorption, which conflicts with the findings of Sokolsky *et al.* (*25*), or that only a small fraction of the total number of surface atoms are active, as the findings of this paper suggest.

From the practical standpoint of commercial fuel cell development, one is primarily interested in the catalytic activity for the oxidation of impure hydrogen, particularly CO/H_2 mixtures. With only 2% CO, even at 160°C, Pt is poisoned to the extent that the reaction rate drops by almost two orders of magnitude (*44*), whereas tungsten carbide is not poisoned by any quantity of CO. Thus, for certain fuel compositions and operating temperatures tungsten carbide may have economic advantages over Pt and the Pt group metals.

ACKNOWLEDGMENTS

The authors thank J. MacDonald for assistance in the electrochemical measurements, Professor M. Svata of the Heyrovsky Institute of Electrochemistry and Dr. H. Boehm of AEG-Telefunken for providing tungsten carbide catalyst samples. We also acknowledge valuable discussions with Drs. L. Bennett and J. Cuthill of the National Bureau of Standards.

REFERENCES

1. Barasel, D., Heidemeyer, J., and Schulz-Ekloff, G., *Bosch. Techn. Ber.* **4**, 35 (1972).
2. Heidemeyer, J., Barasel, D., Gellert, W., and Scharner, P., *Collect. Czech. Chem. Commun.* **36**, 944 (1971).
3. Sarholy, W., and Barasel, D., *Bosch. Tech. Ber.* **4**, 329 (1974).
4. Mund, K., Richter, G., and Von Sturm, F., *Collect. Czech. Chem. Commun.* **36**, 439 (1971).
5. Binder, H., Koehling, A., Kuhn, W., Lindner, W., and Sandstede, G., *Nature (London)* **224**, 1299 (1969).
6. Boehm, H., and Pohl, F., *J. Int. Etudes Piles a Combustile* (Brussels, June 1969), 183–186.
7. Baudendistel, L., Boehm, H., Heffler, J., Louis, G. and Pohl, F., 7th *Int. Energy Conversion Eng. Conf. Proc.* (Washington) *1972*), pp. 20–22.
8. Svata, M., and Zabransky, Z., *Collect. Czech. Chem. Commun.* **39**, 1015 (1974).
9. Svata, M., and Zabransky, Z., *Powder Tech.* **11**, 183 (1975).
10. Von Benda, K., Binder, H., Koehling, A., and Sandstede, G., *in* "From Electrocatalysis to Fuel Cells" (G. Sandstede, Ed.), pp. 87–100. Univ. Washington Press, London, 1972.
11. Binder, H., Koehling, A., and Sandstede, G., Prepr. Papers Presented: New York, N.Y., September 7–12, 1969 (ACS, Washington), Vol. 13, No. 3, Pap. No. 99.
12. Boehm, H., and Baudendistel, L., *Germ. Pat.* 2,106,599, 1972.
13. Levy, R., and Boudart, M., *Science* **181**, 547 (1973).
14. Ross, P., and Stonehart, P., *J. Catal.* **39**, 298 (1975).
15. Ross, P., MacDonald, J., and Stonehart, P., *J. Electroanal. Chem.* **63**, 450 (1975).
16. (a) Bett, J., Kinoshita, K., Routsis, K., and Stonehart, P., *J. Catal.* **29**, 160 (1973). (b) Vogel, W., and Lundquist, J., *J. Electrochem. Soc.* **117**, 1512 (1970).

17. Kuta, J., and Yeager, E., *in* "Techniques of Electrochemistry" (E. Yeager and A. Salkind Eds.), Vol. 1, pp. 141–292. Wiley (Interscience), New York, 1972.
18. X-Ray Powder Diffraction File, ASTM **48-J**, 1960, Sets 1–5.
19. Austin, L., and Lerner, H., *Electrochim. Acta* **9**, 1469 (1964).
20. Vogel, W., Lundquist, J., and Bradford, A., *Electrochim. Acta* **17**, 1735 (1972).
21. Vogel, W., Lundquist, J., Ross, P., and Stonehart, P., *Electrochim. Acta* **20**, 79 (1975).
22. Ross, P., and Stonehart, P., *Electrochim. Acta*, in press (1976).
23. Boehm, H., *Electrochim. Acta* **15**, 1273 (1970).
24. Barasel, D., Gellert, W., Sarholy, W., Schulz–Ekloff, G., *Chem. Ing. Tech.* **13**, 573 (1974); also, Schulz–Ekloff, G., Barasel, D., and Heidemeyer, J., *Collect. Czech. Chem. Commun.* **36**, 928 (1971).
25. Sokolsky, D., Palanker, V., and Baybatyrov, E., *Electrochim. Acta* **20**, 71 (1975).
26. Palmberg, P., Reach, G., Weber, R., and MacDonald, N., (Eds.), "Handbook of Auger Electron Spectroscopy." Physical Electronics Industries, Edina, Minn., 1972.
27. Chung, M., and Jenkins, L., *Surface Sci.* **22**, 479 (1970).
28. Haas, T., and Grant, J., *Appl. Phys. Lett.* **16**, 172 (1970).
29. Coad, J., and Rivere, J., *Surface Sci.* **25**, 609 (1971).
30. Chang, C., *in* "Characterization of Solid Surfaces" (P. Kane and G. Larrabee, Eds.), pp. 534–537. Plenum, New York, 1972.
31. Holloway, P., *J. Vac. Sci. Technol.* **12**, 1418 (1975).
32. Seah, M., *Surface Sci.* **32**, 703 (1972).
33. Powell, C., *Surface Sci.* **44**, 29 (1974).
34. Colton, R., and Rabalais, J., *J. Inorg. Chem.* **15**, 236 (1976).
35. Conklin, J., and Silversmith, D., *Int. J. Quant. Chem.* **25**, 243 (1968).
36. Ramquist, L., *J. Appl. Phys.* **42**, 2112 (1971).
37. Bennett, L., Cuthill, J., McAlister, A., Erickson, N., and Watson, R., *Science* **184**, 563 (1974).
38. Patil, H., and Blakely, J., *J. Appl. Phys.* **45**, 3806 (1974).
39. Palanker, V., Baybatyrov, E., and Sokolsky, D., *Electrochim. Acta* **20**, 51 (1975).
40. Williams, W., Progr. *Solid State Chem.* **6**, 57 (1971).
41. Karchen, W., and Glande, P., *Bien. Conf. Carbon, 11th, 1973*, pp. 43 44.
42. Sturms, E., "The Refractory Carbides," pp. 225–228, 235. Academic Press, New York, 1967.
43. Pourbaix, M., "Atlas of Electrochemical Equilibria in Aqueous Solutions," 1st Engl. ed., p. 282. Pergamon, Oxford, 1966.
44. Stonehart, P., and Ross, P., *Catal. Rev.-Sci. Eng.* **12**, 1 (1975).
45. Voorhies, J., *J. Electrochem. Soc.* **119**, 219 (1972).
46. Trasatti, S., *J. Electroanal. Chem.* **39**, 163 (1972).
47. Ross, P. N., Kinoshita, K., Scarpellino, A., and Stonehart, P., *J. Electroanal. Chem.* **63**, 97 (1975).
48. Ross, P. N., Jr., and Scarpellino, A., unpublished data.